



**HAL**  
open science

## Thermal characterization of polyethylene glycol 600 in liquid, solid phases and through the phase transition

Justine Noel, Yves Jannot, Christel Métivier, Nicolò R Sgreva

### ► To cite this version:

Justine Noel, Yves Jannot, Christel Métivier, Nicolò R Sgreva. Thermal characterization of polyethylene glycol 600 in liquid, solid phases and through the phase transition. 2021. hal-03516867v1

**HAL Id: hal-03516867**

**<https://hal.science/hal-03516867v1>**

Preprint submitted on 7 Jan 2022 (v1), last revised 29 Sep 2022 (v5)

**HAL** is a multi-disciplinary open access archive for the deposit and dissemination of scientific research documents, whether they are published or not. The documents may come from teaching and research institutions in France or abroad, or from public or private research centers.

L'archive ouverte pluridisciplinaire **HAL**, est destinée au dépôt et à la diffusion de documents scientifiques de niveau recherche, publiés ou non, émanant des établissements d'enseignement et de recherche français ou étrangers, des laboratoires publics ou privés.

# Thermal characterization of polyethylene glycol 600 in liquid, solid phases and through the phase transition

Justine Noel, Yves Jannot, Christel Métivier<sup>1</sup> and Nicolò R. Sgreva

---

## Abstract

The polyethylene glycol, a long chain polymer, is characterized by experimental means in both solid and liquid phases. Main thermal properties inherent to the phase transition are also provided in this study. More specifically, we focus on a low molecular weight PEG, named PEG 600, whose average molecular mass is 570-630 g mol<sup>-1</sup> and melting temperature transition is about 10-20°C. The phase change does not occur clearly at a given temperature but rather over a range of temperatures highlighting a complex material. As a first approach, this paper gives thermal properties of the PEG 600 either for completing the literature in which only few properties are provided or for confirming existing data.

Several methodologies have been developed and calibrated in order to obtain in both phases, the density as well as the thermal conductivity. Measurements of the thermal conductivity are carried out using two different methods, i.e. a stationary hot tube device and a transient hot needle one. For the density two different devices are employed for each phase: a densimeter for the liquid phase and a pycnometer for the solid phase. Our results allow to propose a temperature  $T$  dependent fit of density in the liquid phase  $\rho(T) = -0.8164T + 1142.211 \text{ kg.m}^{-3}$ . The relative density variation from the liquid to solid phase is significant as it reaches about 35%, meaning also that the volume shrinkage is quite large. Differential Scanning Calorimetry DSC has been used for measuring the heat capacity of solid and liquid phase as well as the effective one at the transition states. Several protocols have been tested and compared all together in order to characterize intrinsic properties. The latent heat of fusion/solidification has been estimated through the effective heat capacity obtained with heating/cooling protocols. The latent heat converges to one value  $L \approx 130\text{kJ/kg}$ , whatever the protocol used. Undercooling effects are decreased by performing DSC with slow temperature variations. Finally, we have observed several exothermic peaks during

the freezing process highlighting some successive reorganizations within the internal structure of PEG.

---

## 1. Introduction

The polyethylene glycol (PEG) is present in our daily life and covers a wide range of industrial areas, such as cosmetics, pharmaceuticals, food manufacturing, inks. As an example, it is used as a thickener agent in cosmetic products (liquid soaps, moisturizers, shampoos, etc.) and paramedical products (hydro-alcoholic gels, intimate lubricants [1], etc.). It is also used as a solvent in printer inks or to manufacture paint balls, as a food additive and in certain polyester resins. Because it is a bio-compatible product [2], it is also widely used in medical treatments and vaccines [3] such as recently for Covid-19 vaccine. In addition, the polyethylene glycol presents remarkable properties, especially from chemical viewpoint since it is a stable, non corrosive, non toxic product ; and thermal properties such as a large latent heat. A significant advantage lies in the large variety of the temperature transition values which depend on the PEG molecular weight. For instance, phase transition occurs around 15-20°C for the PEG 600, 38-40°C for the PEG 1000 [4], around 44°C for the PEG 1500 [5]. For these reasons, numerous studies have been devoted to propose Composite Phase Change Materials (CPCM) based on polyethylene glycol [6, 7, 8, 9, 10, 11, 12]. Phase change materials (PCM) are widely studied in the field of energy storage/release since a large amount of energy can be transferred during the phase change via the latent heat. Energy is stored during endothermic transformations (e.g. solid to liquid) while it is released during the reversible exothermic transformations. The high latent heat of the PEG makes it a very interesting and attractive PCM. Furthermore, it matches perfectly to the criteria related to the choice of PCM such as low cost, non-toxic, non-flammable, non-corrosive and biodegradable (bio-compatible), i.e. eco-friendly. The uses of PEG in Composite PCM can concern thermal regulation in buildings [13] or pavements [8] as well as in photovoltaic panels [4, 12].

Despite the wide use of PEG, only few papers were devoted to characterize thermal properties of the polyethylene glycol alone. Recently, Kou et al. [14] have measured heat capacities of PEG for molar mass varying from 2000 to 20 000 g mol<sup>-1</sup>. For smaller molar mass such as the PEG 600 (about 570-630 g/mol), few studies have been dedicated to characterize its thermal

properties. Data available in the literature correspond mainly to properties in the liquid phase. Some density measurements are provided by several authors [15, 16, 17, 18], but the data is only given in the liquid phase for few temperature values, not sufficient to obtain the thermal expansion coefficient.

In a paper dedicated to properties of PCM, Lane [19] presents some properties for numerous PCM, including PEG 600. For this specific PCM, the author indicates the melting point (22°C), the thermal conductivity in liquid phase for only two temperature values (38.6°C and 67°C), the density in liquid phase at 25°C and the latent heat of melting. Some other studies present the thermal conductivity of liquid phase [17, 19]. Finally, the properties of PEG remain partial and scattered in the literature. Moreover, the small number of measured properties is only obtained in the liquid phase. To our knowledge, the latent heat of solidification, the freezing point, the thermal conductivity, the density and the heat capacity in the solid phase are not available in the literature.

From a structural viewpoint, the PEG properties - particularly at the solid-to-liquid transition - depend on the molecular weight and also on the protocols involved. Several types of aggregates structures, such as helical or spherical conformations have been observed within the freezing process [20, 21]. However, to our knowledge, no real consensus is proposed in the literature to correlate clearly the structure with experimental conditions. This is of importance since the structural organization can have a significant impact on the macroscopic properties. For instance, re-organization of crystals in the solidification process leads to different intensities and/or peaks of exothermic transformations, thus different values of heat transfer as observed by Differential Scanning Calorimetry DSC for several semicrystalline polymers [20, 22].

As a first step in the understanding of PEG behaviour related to conditions of use, we propose to clarify and provide new macroscopic properties of a PEG with a low molecular weight, i.e. the PEG 600. The aim of our study is to characterize this polyethylene glycol in both the solid and liquid phases. In the liquid phase, we propose measurements in order to validate and refine properties with temperature providing original values. In the solid phase, we aim to fill the data gap in the literature. This present article presents detailed methodologies and protocols used for characterizing the main PEG thermal properties in each phase: the density, the effective heat capacity and the conductivity ; and the latent heat of melting and solidification. First, the different methodologies and detailed protocols are presented in section

2, then the results are provided in section 3. They are compared with the properties available in the literature. This paper ends with conclusions and perspectives.

## 2. Methods and experimental devices

### 2.1. Material

Polyethylene glycol (PEG) is a linear polyether made from ethylene glycol monomers characterized by a molar mass smaller than 20 000 g mol<sup>-1</sup> in general. In this study, we aim at characterizing a low molecular weight polyethylene glycol, named PEG 600, supplied by Merck (CAS 25322-68-3). Several batches have been used to verify reproducibility of results. This material corresponds to a long chain polymer with a molecular weight of around 570-630 g mol<sup>-1</sup>. The temperature of the solid-liquid phase change is indicated by the supplier within the range of 17-22 °C.

### 2.2. Density

#### 2.2.1. Liquid phase

The density ( $\rho$ ) of PEG 600 in liquid phase is measured by using a Densimeter DMA 5000M, Anton Paar. The densimeter provides a 10<sup>-6</sup> g cm<sup>-3</sup> accuracy in the temperature range of 0-60 °C, while for larger temperatures (up to a maximum of 100 °C) the accuracy decreases to 10<sup>-4</sup> g cm<sup>-3</sup>. The precision on the temperature is 0.01 °C. Density measurements are carried out at constant pressure  $P$  (atmospheric pressure) and within the temperature range of 21-100 °C in which PEG 600 is liquid.

Within this framework, the time to achieve the thermal stability is about 5 minutes per temperature step. To ensure reproducible results, density is measured on three different samples (volume of  $\sim$ 1 mL) from two different batches. At a given temperature, the maximal variation between measurements is 10<sup>-4</sup> g cm<sup>-3</sup> and the final value of density is taken as the mean of these measurements. From the temperature dependence of the density, we evaluate the thermal expansion coefficient  $\beta$  as follows

$$\beta = -\frac{1}{\rho_0} \left( \frac{\partial \rho}{\partial T} \right)_P, \quad (1)$$

with  $\rho_0 = \rho(T_0)$  being a reference density defined at the reference temperature  $T_0$ . The thermal expansion coefficient indicates the first-order density

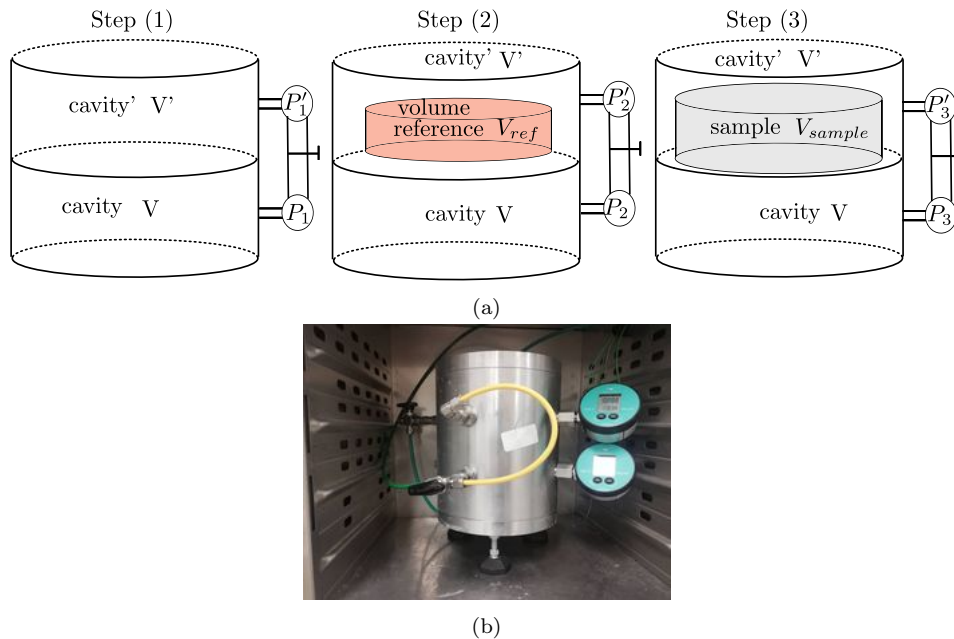


Figure 1: (a) Sketch and (b) photo of pycnometer

variations with temperature (Boussinesq approximation) at constant pressure [23] and, for a given mass of a material, it also corresponds to the volume variation with temperature.

### 2.2.2. Solid phase

Density measurements in the solid phase have been achieved using a lab-made pycnometer. The device is placed in a thermostatic enclosure Binder<sup>TM</sup> KBF 115 in order to control the temperature.

The pycnometer consists in two different cavities of volume  $V$  and  $V'$  separated by a valve as represented in Fig. 1. The measurement procedure consists in first obtaining the vacuum in both cavities  $P' = P = 0$ , then the valve is closed and a pressure  $P'_i$  is imposed to the lower cavity. The valve is then opened involving pressure variations until an equilibrium is reached within the two cavities leading to a final pressure  $P_f$ . The pressure is measured using a Mano 2000 Leo 3 Keller with an accuracy of 1 mbar. We first started by measuring the volumes  $V$  and  $V'$  of each cavity by repeating several times the above mentioned procedure through Steps (1) and (2) as

Step (1)			Step (2)		
$P_i$ (bar)	$P_f$ (bar)	$P_f/P_i$	$P_i$ (bar)	$P_f$ (bar)	$P_f/P_i$
3.654	1.685	46.1%	3.655	2.002	54.7%
3.660	1.696	46.3%	3.650	2.002	54.8%
3.665	1.706	46.5%	3.603	1.976	54.8%

Table 1: Pressure measurements performed for Steps (1) and (2)

named in Fig. 1 a.

Pressure measurements are summarized in Table 1. Each Step is repeated 3 times, the Table 1 highlights a good stability in terms of pressure values within 0.4 % of variation in results.

The calibration of the device was then performed using a stainless steel sample with a known volume of  $3.92 \times 10^{-5} \text{ m}^3$  (step (3) in Fig. 1 a). According to the following equation :

$$P_i V = P_f \times (V + V' - V_{sample}), \quad (2)$$

the measurements led to a volume  $V_{sample} = 3.82 \times 10^{-5} \text{ m}^3$ , i.e. within 2.6 % difference with the calibrated value. This value has been obtained by repeating several times this step (at least 4 times).

This same protocol is performed with a given mass of PEG. The temperature set in the binder is 0.5 °C in order to have a fully solid PEG sample. Finally, the density of PEG in solid phase is deduced from the volume measurements.

### 2.2.3. Liquid phase

The thermal conductivity of the liquid phase is measured via a device related to the stationary hot tube method developed at the laboratory [24] as represented in Fig. 2. The material is introduced in the liquid phase into the gap (between radii  $r_1$  and  $r_2$ ) of two coaxial cylinders made respectively of copper and stainless steel for the outer and inner cylinders. An electric current  $I$  is applied to the inner cylinder, producing heat flux by Joule effect. The outer part of the copper cylinder is maintained at a given temperature via a temperature controlled water flow. The temperatures  $T_1$  and  $T_2$  are measured using two type K thermocouples stuck on the wall of the tubes, i.e. at the boundaries of the liquid layer (see also Fig. 2). In order to avoid any up-down wall effects, thermocouples are located at the mid-height of

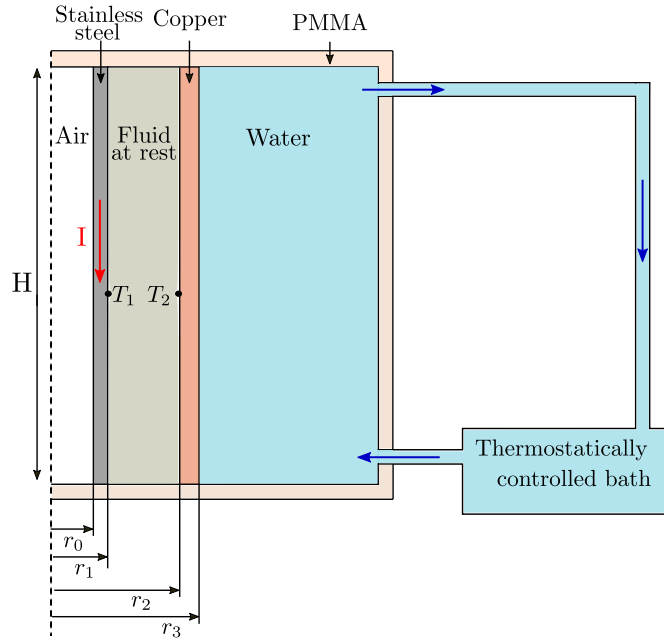


Figure 2: Hot tube device: thermal conductivity measurements -  $r_0 = 2.54\text{mm}$ ,  $r_1 = 2.75\text{mm}$ ,  $r_2 = 6.00\text{mm}$

the device. The temperature difference is measured thanks to the voltage difference  $U$  between these two thermocouples (type K):

$$\Delta T = T_1 - T_2 = U/k,$$

where  $k$  is a thermocouples specific constant given in our case by  $k = (39.2 + 0.064 \times T_2 - 0.005 \times T_2^2) \times 10^{-6}$  ( $\text{V K}^{-1}$ ). Thermocouples are connected to a cold junction block. The tension is measured with Keysight U3401A 4 1/2 Digit Dual Display Multimeter.

Provided that the regime is only conductive in the liquid layer (fluid at rest), the thermal conductivity can be deduced as follows (Jannot & Degiovanni [24]):

$$\lambda = \frac{\rho_{el} I^2 \ln(r_2/r_1)}{2\pi^2(r_1^2 - r_0^2)\Delta T} \quad (3)$$

with  $\rho_{el} = 7.3 \cdot 10^{-7}(1 + 1.36 \times 10)^{-2}(T - T_{ref})$  the electrical resistivity of the stainless steel and  $T_{ref}$  a temperature reference set to  $20^\circ\text{C}$ .

The dimensions of the device were determined under the condition that no convection occurs for a large range of liquids. According to Huetz [25],

we ensure that the following condition is satisfied:

$$\frac{Ra}{H^+} < 400 \quad (4)$$

where  $H^+ = H/\delta$ ,  $H$  is the height of cylinders,  $\delta = r_2 - r_1$  is the thickness of the liquid layer and  $Ra$  corresponds to the Rayleigh number given by

$$Ra = \frac{\rho g \beta \Delta T \delta^3}{\mu a}, \quad (5)$$

with  $\mu$  being the dynamic viscosity and  $a$  the thermal diffusivity of the fluid.

This condition is verified a posteriori and in the case of our measurements carried out with PEG we estimate to  $Ra/H^+ \approx 15 - 20 \ll 400$ .

The validation of the device was done with water, measurements led to a maximal difference in thermal conductivity of 2 % compared with values provided by Brown & Marco [26]. Since the device is filled by the PCM in liquid phase, the volume of the sample varies with the temperature, the largest variation occurring during the phase transition. As it is for the majority of materials, PEG decreases in volume going from the liquid to the solid phase. This can lead to imperfect contacts during the solidification at walls as detailed in Appendix A Appendix A. It means that this device is unsuitable for measuring thermal conductivity of materials in solid phase if such conditions occur, i.e. thermal contact resistance at walls. For this reason, we propose another technique to carry out measurements in the solid phase. This technique is detailed in the following paragraph.

#### 2.2.4. Hot needle method

We developed a specific device in order to measure the thermal conductivity of any material in solid or liquid phases. The device consists in a cavity made of PMMA whose dimensions are  $200 \times 120 \times 120 \text{ mm}^3$ . A hollow needle -  $r_i = 0.8 \text{ mm}$  and  $r_e = 1.25 \text{ mm}$ , respectively the inner and outer radii - heated by Joule effect is placed in at the center of the device. Its corresponding heat flow rate per unit length  $L$  is  $\phi = \frac{RI^2}{L}$ , with  $R$  the electrical resistivity and  $I$  the electric intensity. Inside the needle, the temperature is measured with a type K sheath thermocouple whose radius is  $r_t = 0.5 \text{ mm}$ . The needle is made of stainless steel and its length is  $L = 300 \text{ mm}$  larger

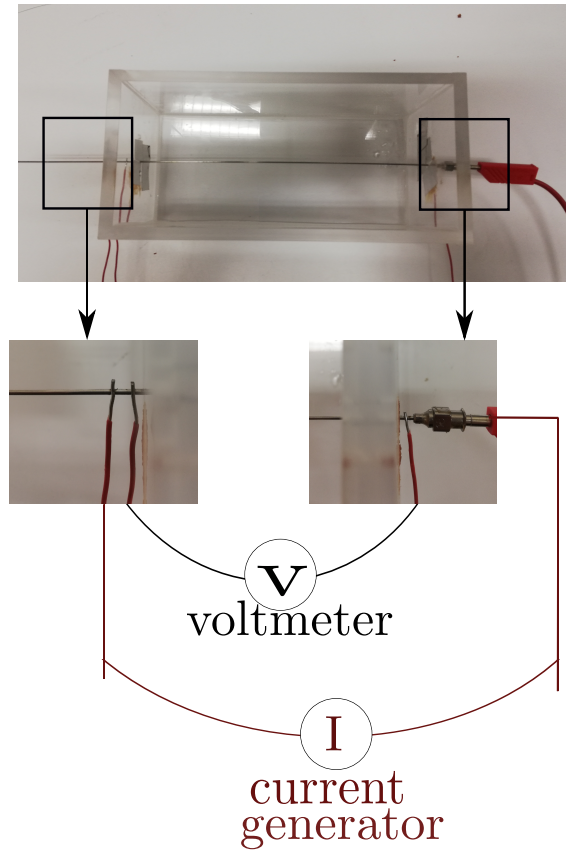


Figure 3: Photo of the heated needle device

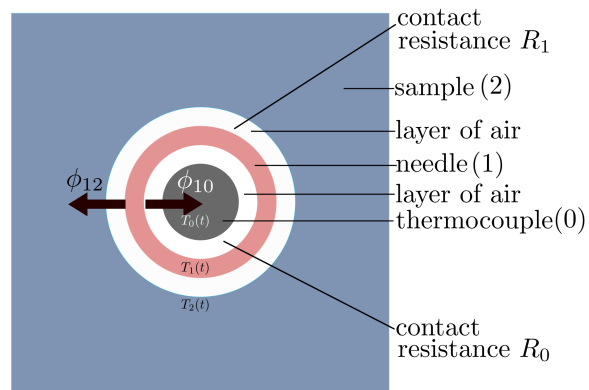


Figure 4: Schematic cross section view of the needle probe device.

than the cavity as can be seen in the photo of the device (Fig. 3). Temperature measurements are done inside the needle at the center of the cavity. Temperatures are recorded using a TC-08 Picolog device with a frequency of 10 Hz. The cavity is filled by the material, here the PEG 600. Contacts at interfaces, i.e. needle (1) - material (2) ; and needle (1) - thermocouple (0), being not perfect, it results in thermal contact resistances  $R_1$  and  $R_0$  respectively, as sketched in Fig. 4. These contact resistances are taken into account in what follows.

Here again, the device is placed in a Binder<sup>TM</sup> KBF 115 thermostatic chamber in order to maintain the system at a controlled temperature. The device is left in the Binder long time enough to reach a constant initial temperature in the whole system, and more specifically in the thermocouple, needle and PEG, that is to say  $T_0(0) = T_1(0) = T_2(0)$ . Furthermore, the cavity being long enough, we consider a unidirectional dependence of parameters at the center of the cavity. On the other hand, we assume uniform temperature fields  $T_1(t)$  and  $T_0(t)$  in the needle and thermocouple respectively since they are very thin. As the needle is heated, the total heat flow rate  $\phi$  due to Joule effect can be splitted into  $\phi_{12}$  (heat transferred to the material) and  $\phi_{10}$  (heat transferred to the thermocouple), such as  $\phi = \phi_{10} + \phi_{12}$ . Furthermore, heating the needle would also induce transient variations in temperature within the whole system. Thermal properties of PEG can be obtained by considering heat equation in two domains (conductive regime) assorted with boundary conditions. For this purpose, we use the quadrupole formalism as proposed by Maillet *et al.*.

The first domain is bounded by the outer surface of the needle ( $r_1 = r_e (\approx r_i)$ ) and a surface of the material sample ( $r_2 \rightarrow \infty$ ). Following the method proposed by Maillet, the thermal quadrupole formalism writes:

$$\begin{bmatrix} \theta_1 \\ \Phi_{12} \end{bmatrix} = [M1][M2] \begin{bmatrix} \theta_2 \\ \frac{\theta_2}{Z} \end{bmatrix} = \begin{bmatrix} 1 & 0 \\ C_1 p & 1 \end{bmatrix} \begin{bmatrix} 1 & R_1 \\ 0 & 1 \end{bmatrix} \begin{bmatrix} \theta_2 \\ \frac{\theta_2}{Z} \end{bmatrix} = \begin{bmatrix} 1 & R_1 \\ C_1 p & 1 + R_1 C_1 p \end{bmatrix} \begin{bmatrix} \theta_2 \\ \frac{\theta_2}{Z} \end{bmatrix} \quad (6)$$

with:

$\theta_1 = \mathcal{L}(T_1(t) - T_1(0))$  the Laplace transform of the needle temperature variation  $[T_1(t) - T_1(0)]$ ,

$\theta_2 = \mathcal{L}(T_2(t) - T_2(0))$  the Laplace transform of the material temperature variation at the interface needle/material  $[T_2(t) - T_2(0)]$ ,

$\Phi_{12} = \mathcal{L}(\phi_{12})$  the Laplace transform of  $\phi_{12}$ ,

$M1$  the quadrupolar matrix representing the needle as a pure capacity  $C_1$ ,  
 $M2$  the quadrupolar matrix representing the contact resistance at interface (1)-(2),

$$C_1 = \pi(r_e^2 - r_i^2)\rho_1 c_1, \quad (7)$$

$$Z = \frac{K_0(qr_e)}{2\pi\lambda qr_e K_1(qr_e)}, \quad (8)$$

$$q = \sqrt{\frac{p}{a}} \quad (9)$$

$p$  the Laplace parameter ( $s^{-1}$ ),

$\rho_1$  the density of the needle ( $\text{kg m}^{-3}$ )

$c_1$  the specific heat of the needle ( $\text{J K}^{-1} \text{kg}^{-1}$ )

$R_1$  the thermal contact resistance per unit of length at the interface (1)-(2) ( $\text{m K W}^{-1}$ )

$a$  the thermal diffusivity of the sample ( $\text{m}^2 \text{s}^{-1}$ )

$\lambda$  the thermal conductivity of the sample ( $\text{W m}^{-1} \text{K}^{-1}$ ).

Similarly, we consider a second domain bounded by the thermocouple  $r_0 = 0 (\approx r_t)$  and the inner needle surface  $r_1 = r_i (\approx r_e)$ . The quadrupole formalism leads to:

$$\begin{bmatrix} \theta_1 \\ \Phi_{10} \end{bmatrix} = [M3][M4] \begin{bmatrix} \theta_0 \\ 0 \end{bmatrix} = \begin{bmatrix} 1 & R_0 \\ 0 & 1 \end{bmatrix} \begin{bmatrix} 1 & 0 \\ C_0 p & 1 \end{bmatrix} \begin{bmatrix} \theta_0 \\ 0 \end{bmatrix} = \begin{bmatrix} 1 + R_0 C_0 p & R_0 \\ C_0 p & 1 \end{bmatrix} \begin{bmatrix} \theta_0 \\ 0 \end{bmatrix} \quad (10)$$

with:

$\theta_0 = \mathcal{L}(T_0(t) - T_0(0))$  the Laplace transform of the thermocouple temperature variation  $[T_1(t) - T_1(0)]$ ,

$\Phi_{10} = \mathcal{L}(\phi_{10})$  the Laplace transform of the heat flow rate  $\phi_{10}$ ,

$M3$  the quadrupolar matrix representing the contact resistance at interface (0)-(1),

$M4$  the quadrupolar matrix representing the thermocouple as a pure capacity  $C_0$ ,

$$C_0 = \pi r_t^2 \rho_0 c_0 \quad (11)$$

$\rho_0$  the density of the thermocouple ( $\text{kg m}^{-3}$ )

$c_0$  the specific heat of the thermocouple ( $\text{J K}^{-1} \text{kg}^{-1}$ ).

$R_0$  the thermal contact resistance per unit length between the thermocouple and the needle ( $\text{m K W}^{-1}$ )

We deduce:

$$\theta_1 = \left(1 + \frac{R_1}{Z}\right) \theta_2 \quad (12)$$

$$\Phi_{12} = \left(C_1 p + \frac{1 + R_1 C_1 p}{Z}\right) \theta_2 = \left(C_1 p + \frac{1 + R_1 C_1 p}{Z}\right) \frac{\theta_1}{1 + \frac{R_1}{Z}} \quad (13)$$

$$\theta_1 = (1 + R_0 C_0 p) \theta_0 \quad (14)$$

$$\Phi_{10} = C_0 p \theta_0 = \frac{C_0 p}{1 + R_0 C_0 p} \theta_1 \quad (15)$$

The Laplace transform of the total heat flow rate  $\phi$  writes:

$$\mathcal{L}(\phi) = \frac{\phi}{p} = \Phi_{10} + \Phi_{12} = \left(\frac{Z C_1 p + 1 + R_1 C_1 p}{Z + R_1} + \frac{C_0 p}{1 + R_0 C_0 p}\right) \theta_1 \quad (16)$$

$$\theta_0 = \frac{\phi}{p} \frac{Z + R_1}{(Z + R_1)[(C_0 + C_1)p + R_0 C_0 C_1 p^2] + 1 + R_0 C_0 p} \quad (17)$$

At long time ( $p \rightarrow 0$ ), equations simplify to:

$$\theta_0 = \frac{\phi}{p} (Z + R_1) \quad (18)$$

$$K_0(qr_e) = -\ln\left(\frac{qr_e}{2}\right) - \gamma \quad (19)$$

$$K_1(qr_e) = \frac{1}{qr_e} \quad (20)$$

$$\theta_0(p) = \frac{\phi}{p} \left[ -\frac{\ln\left(\frac{qr_e}{2}\right)}{2\pi\lambda} - \frac{\gamma}{2\pi\lambda} + R_1 \right] \quad (21)$$

$$= \frac{\phi}{p} \left[ -\frac{\ln(p)}{4\pi\lambda} - \frac{\ln\left(\frac{r_e}{2\sqrt{a}}\right)}{2\pi\lambda} - \frac{\gamma}{2\pi\lambda} + R_1 \right] \quad (22)$$

By performing the inverse Laplace transform, we obtain:

$$T_0(t) = \phi \left[ \frac{\ln(t)}{4\pi\lambda} + \frac{\gamma}{4\pi\lambda} - \frac{\ln\left(\frac{r_e}{2\sqrt{a}}\right)}{2\pi\lambda} - \frac{\gamma}{2\pi\lambda} + R_1 \right] \quad (23)$$

$$T_0(t) = \frac{\phi}{4\pi\lambda} \ln(t) + \phi \left( \frac{-\gamma}{4\pi\lambda} - \frac{\ln\left(\frac{r_e}{2\sqrt{a}}\right)}{2\pi\lambda} + R_1 \right) \quad (24)$$

Equation (24) highlights a logarithm dependency with time which becomes the dominant term at long times. This equation is valid provided that the regime remains conductive and the medium is infinite. Hence, we write :

$$T_0(t) = D_1 + D_2 \times \ln(t) \quad (25)$$

with  $D_1$  and  $D_2$  two constants which depend on the material's thermal conductivity  $\lambda$ . Temperature measurements allow to identify these two parameters by minimising:  $S = \sum_{t_d}^{t_f} (T_{exp}(t) - T_0(t))^2$  on a time interval  $[t_d, t_f]$ . The thermal conductivity is finally obtained by evaluating the following equation:

$$\lambda = \frac{\phi}{4\pi D_2} \quad (26)$$

### 2.3. Specific heat capacity and latent heat

The specific heat capacity  $c_p$  as well as the latent heat of the material are obtained using a Setaram  $\mu$ dSc3 differential calorimeter.

The protocol consists in applying temperature variations to the sample (sample mass about 200 - 300 mg) measuring simultaneously heat transfer along time. In this present study, temperature variations correspond to ramps of different rates of cooling/heating ( $1^\circ\text{C min}^{-1}$ ,  $0.5^\circ\text{C min}^{-1}$ ,  $0.2^\circ\text{C min}^{-1}$ ) as well as temperature steps leading to quasi-steady thermal conditions. For this purpose, steps last long time enough in order to recover a steady state, i.e. no more heat flux between the sample and the device. In practice, it corresponds to a minimum of 1 hour up to 2 hours per temperature step. Increments between temperature steps are set to  $1^\circ\text{C}$  when phase change occurs, i.e. between  $10^\circ\text{C}$  and  $30^\circ\text{C}$ , in order to gain in accuracy in the evaluation of the effective  $c_p(T)$  and of the phase change temperature interval. Outside this temperature range, the increment is  $2^\circ\text{C}$ . In any case, the

increment between two successive steps is obtained applying a temperature ramp of  $0.2 \text{ }^\circ\text{C min}^{-1}$ .

Long time steps or slow temperature variations have the advantage to avoid, at least to minimize undercooling effects. Reversibility of results are tested performing the entire protocol by increasing and decreasing temperature values. The effective heat capacity is deduced from the heat transferred to the sample subjected to temperature variations. At the phase transition, the equivalent  $c_P$  varies strongly corresponding to sensible heat plus an additional part due to latent heat. Subtracting the sensible heat obtained from liquid and solid phases respectively, we can estimate the latent heat.

### 3. Results

#### 3.1. Density

##### 3.1.1. Liquid phase

Density measurements of PEG 600 are presented in Fig. 5 in the temperature range  $25^\circ\text{C}$ - $100^\circ\text{C}$ . Measurements have been performed by cooling (decreasing the temperature) in order to avoid any troubles such as bubbles due to heating (large temperature range) or a mushy phase as an initial state (close to  $25^\circ\text{C}$ ). This precaution enables to obtain reproducible density values under our experimental conditions.

Our experimental values are summarized in Fig. 5 in which values obtained in the literature [18, 15, 16] have been added. We observe a very good agreement in results as also confirmed in Table 2. Our results are included within a maximal difference of 1 % with the above cited studies. Our results can be fitted by a linear model (continuous line in Fig. 5) as follows:

$$\rho(T) = -0.81643 \times T + 1142.2114 \text{ kg m}^{-3} \quad (27)$$

with  $T$  here is the temperature in  $^\circ\text{C}$ .

Furthermore, the thermal expansion coefficient  $\beta$  can be evaluated according to Eq. (1). For instance around  $T_0 = 25 \text{ }^\circ\text{C}$ , we obtain  $\rho_0 = \rho(T_0) = 1121.96 \text{ kg m}^{-3}$  and  $\beta = 7.28 \times 10^{-4} \text{ K}^{-1}$ .

##### 3.1.2. Solid phase

The density of PEG in solid phase is obtained using the lab-made pycnometer as described in section 2.2.2. We introduce a given mass of PEG sample (about  $m \approx 150 \text{ g}$ ) into the upper cavity and let the pycnometer

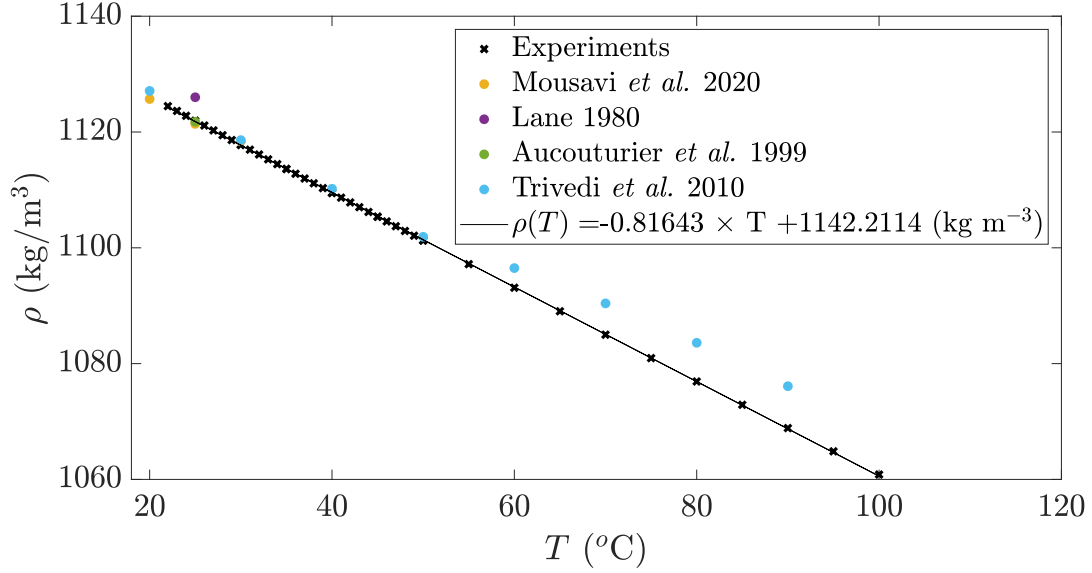


Figure 5: Density  $\rho$  of PEG 600 as a function of temperature.

T( °C)	Density $\rho \times 10^3$ (kg.m <sup>-3</sup> )		
	Exp.	Lit.	Deviation %
20	1.127156	1.1257 [18]	-
25	1.121956	1.126 [19]	0.36
		1.1214 [18]	0.05
		1.12177 [15]	0.02
30	1.117763	1.1184 [18]	0.06
		1.1186 [16]	0.07
40	1.109468	1.1102 [16]	0.07
50	1.101259	1.1019 [16]	0.06
60	1.093104	1.0965 [16]	0.31
70	1.084992	1.0904 [16]	0.50
80	1.076914	1.0836 [16]	0.62
90	1.068864	1.0761 [16]	0.67

Table 2: Density  $\rho$  of the PEG 600 at different temperature values - Comparison with values given in literature

First set			Second set		
$P_i$ (bar)	$P_f$ (bar)	$P_f/P_i$	$P_i$	$P_f$	$P_f/P_i$
3.317	1.816	54.7%	3.555	1.943	54.6%
3.266	1.788	54.7%	3.365	1.851	54.7%
3.415	1.869	54.7 %	3.296	1.807	55 %
3.548	1.938	54.7%	3.399	1.861	54.8%

Table 3: Pressure measurements performed for different samples of PEG 600.

24h into the oven at 0.5°C before performing any measurement to ensure a complete solidification of PEG. Measurements are performed into the oven at the same temperature 0.5°C. They are repeated 4 times per sample. Several batches of PEG sample have been tested. Typical pressure measurements are provided in Table 3, we observe a good agreement in results when changing the sample as we observed.

The density of PEG in solid phase is then evaluated, leading to the value  $\rho = 1510 \pm 23 \text{ kg m}^{-3}$  at 0.5°C. This value is quite different from the one obtained in the liquid phase. However, it is not surprising as it is correlated to large variations in volume during solidification.

### 3.2. Thermal conductivity

#### 3.2.1. Liquid phase - Steady hot tube method

As above mentioned in section 3.2.1, this method is relevant only in the liquid phase as it leads to good thermal contacts between the liquid and tubes surfaces. Since we fill the device with PEG in liquid phase, the largest decrease in volume is observed at the liquid to solid transition leading to thermal resistances at interfaces.

Above 20°C, the PEG600 is liquid and we assume negligible surfaces contact resistance. Below this temperature, we have observed that results are no longer reproducible due to the liquid-to-solid transition. Measurements are performed at steady state. Results obtained with this device are presented in Fig. 6 ('+' symbols) as a function of the mean temperature  $\bar{T} = T = \frac{T_1 + T_2}{2}$ . Additional values of thermal conductivity given by Lane [19] and values given by Dynalene in a data sheet product have been added in Fig. 6 for comparison. Within our experiments, the temperature variation  $\Delta T = T_2 - T_1$  does not exceed 3°C through the annular region, i.e. between  $r_1$  and  $r_2$ . In the range of the tested temperatures, we observe a slight tem-

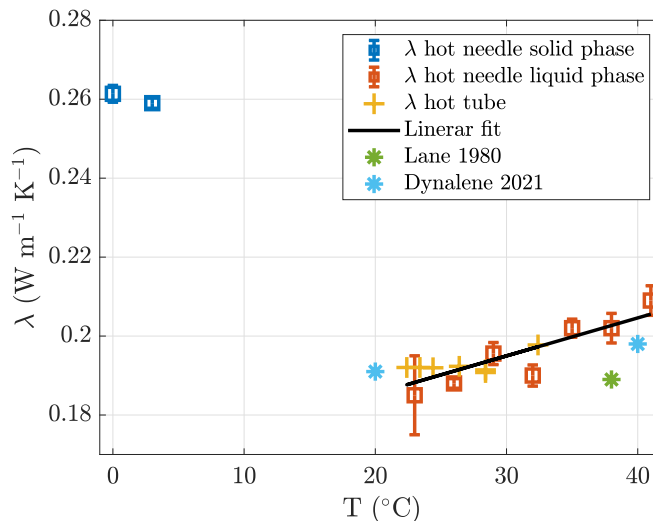


Figure 6: Conductivity results for liquid phase and solid phases

perature dependence  $\lambda$ . These measurements are completed in the liquid and solid phases using the hot needle method.

### 3.2.2. Solid and liquid phases - Hot needle method

The measurements are carried out with the needle probe described previously in Section 2.2.4. The estimation of the thermal conductivity  $\lambda$  is realized assuming conductive regime in the vicinity of the needle, an infinite medium and a  $T(t) \propto \ln(t)$  dependency at long time. The time interval  $[t_i, t_f]$  corresponding to this latter condition is determined empirically in such a way that the difference between experiments and the model is close to zero (see the discussion below about residuals).

Thermal conductivity values in the solid phase are obtained placing the device in the temperature controlled binder. An example of temperature measurements are plotted in Fig. 7 as a function of time. In the same figure, we have also displayed temperature values estimated by the model given by Eq. (24). Residuals multiplied by 10 are also plotted in order to compare both measurements with the model. For each set of experiments, we determine the time interval  $[t_i, t_f]$  along which residuals are perfectly flat and centered on zero, i.e. in which interval our model is consistent. This interval is bounded by vertical lines in Figs. 7 and 8. In the case presented in Fig. 7, the estimation interval was adjusted to  $[20 \text{ s}, 1000 \text{ s}]$ . The divergence of the residuals after 1000 s indicates the limit of validity of the semi-infinite

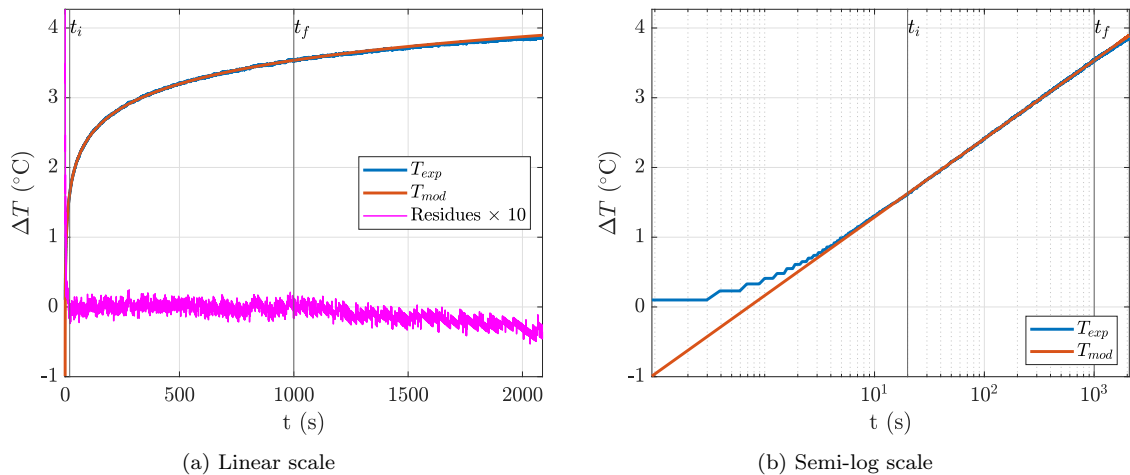


Figure 7: Experimental and simulated curves with the simplified model and estimation residues 10 for solid PEG at 3 °C with the hot needle method

medium assumption. Within the estimation interval we evaluate  $D_2$  (see eq. 25) the slope of temperature variations with time in a semi log scale (fig. 7b).

The model remains valid in the liquid phase provided that no convection occurs. Under this condition, we have also performed some measurements above 20°C. Typical results are provided in Fig. 8, they represent the experimental and simulated temperature variations along time assuming similar conditions as above mentioned. Residuals multiplied by 10 are also plotted. Figure 8 corresponds to two different temperatures imposed in the binder, i.e. 26°C and 41°C. The estimation interval was adjusted to [50 s, 300 s] for the measurement at 26 °C and to [20 s, 60 s] for the measurement at 41 °C. The residuals are found to be flat and centered on zero over these intervals. The divergence of the residuals after 60 s, in the case of 41 °C, is explained by the occurrence of convection around the needle. The higher the temperature is, the earlier this phenomenon appears; for instance convection is not observed before 300 s at 26 °C.

Figure 6 summarizes all the thermal conductivity measurements as a function of the temperature in the case of PEG 600. Values obtained via the needle method (squares) are consistent with the ones obtained using the hot tube method in the liquid phase. They are also in good agreement with values proposed in the literature.

The thermal conductivity in liquid phase presents a slight increase with

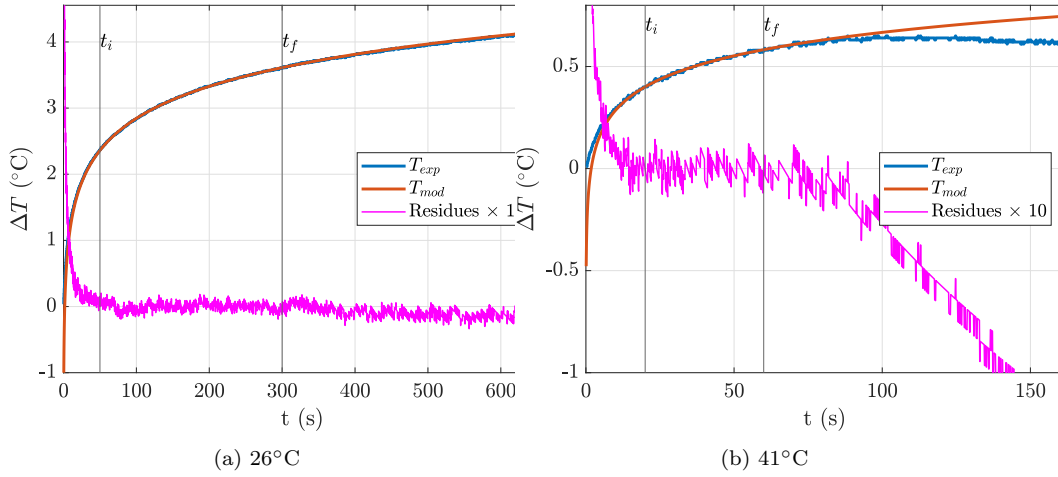
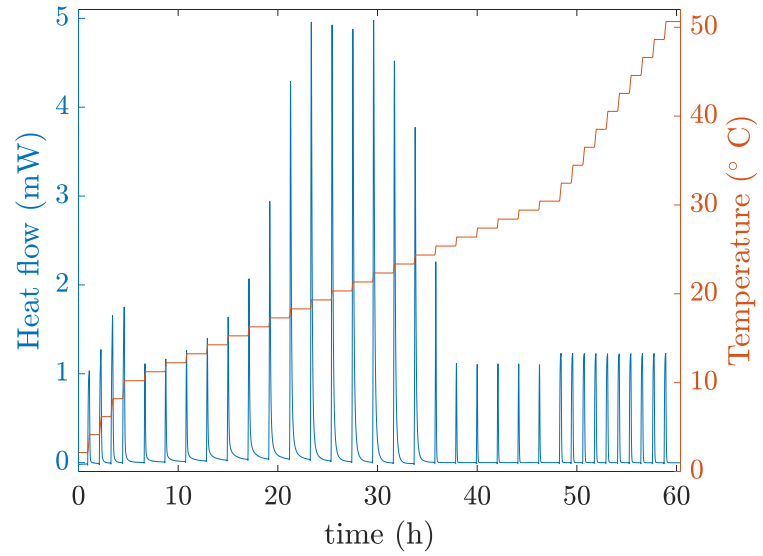


Figure 8: Experimental and simulated curves with the simplified model and estimation residuals 10 for liquid PEG at 26 °C and 41 °C with the hot needle method

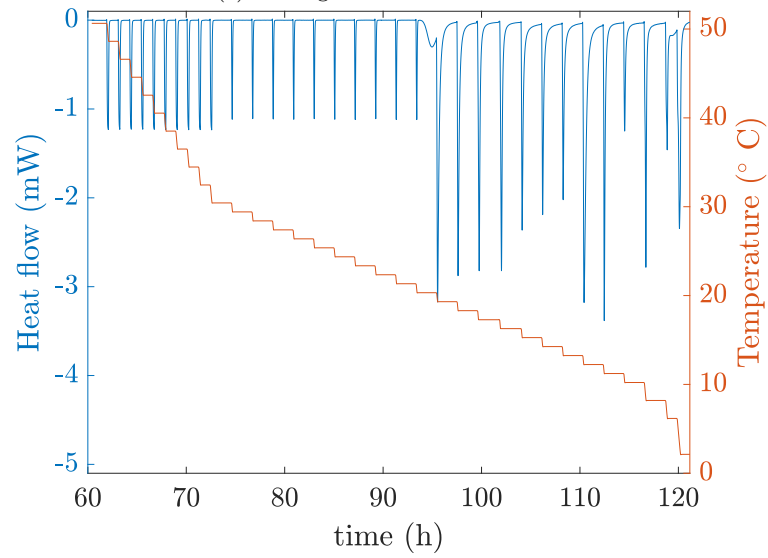
temperature following a linear variation:

$$\lambda(T) = 0.1554 + 0.001267 \times T$$

with  $\lambda$  in  $\text{W m}^{-1} \text{K}^{-1}$  and the temperature  $T$  in  $^{\circ}\text{C}$ . Our results are also very close to those given by Dynalene in a data sheet product:  $\lambda = 0.191 \text{ W m}^{-1} \text{K}^{-1}$  at  $20^{\circ}\text{C}$  and  $\lambda = 0.198 \text{ W m}^{-1} \text{K}^{-1}$  at  $40^{\circ}\text{C}$  and they are comparable to those published by Lane [19] who obtained  $\lambda = 0.189 \text{ W m}^{-1} \text{K}^{-1}$  at  $38^{\circ}\text{C}$  and  $\lambda = 0.187 \text{ W m}^{-1} \text{K}^{-1}$  at  $67^{\circ}\text{C}$ . The value of conductivity in solid phase, i.e.  $0^{\circ}\text{C}$  and  $3^{\circ}\text{C}$ , does not vary much in this temperature range leading to  $\lambda_s \approx 0.260 \text{ W m}^{-1} \text{K}^{-1}$ . It is quite difficult to increase the range of temperature measurements since, at  $6^{\circ}\text{C}$ , the temperature near the needle is around  $10^{\circ}\text{C}$  and the material starts to melt. Hence the gap between  $3^{\circ}\text{C}$  and  $20^{\circ}\text{C}$  in terms of thermal conductivity is explained by a phase transition within a large temperature range. Finally, our measurements provide values of thermal conductivity in each liquid and solid phases. An effective value of  $\lambda$  could be measured in the temperature range  $3^{\circ}\text{C}$  to  $20^{\circ}\text{C}$ , however we really think that investigating the material structure at the phase transition would be more relevant. This aspect is beyond the scope of this present article. It would be investigated in a close future.



(a) Melting



(b) Solidification

Figure 9: Heat flow rate (blue) measurements in the case of PEG 600 for (a) increasing and (b) decreasing temperature steps (red).

### 3.3. Specific capacity and latent heat

Raw data obtained by differential scanning calorimetry is presented in Fig. 9 in the case of imposed temperature steps (in red). This figure displays the heat flux (in blue) transferred between the PCM sample and the calorimeter. We observed that each increment leads to a peak in terms of heat which goes back to zero as a thermal equilibrium is reached. From this experimental protocol, the effective heat capacity is deduced by integrating the heat flux over the time (including the increment) of one step and dividing by the sample mass  $m$  and the temperature increment.

For temperature ramps, i.e. continuous temperature variations with time, we directly determine the effective  $c_p$  from experimental measurements of the heat flux  $\phi$  according to the following equation:

$$\phi = mc_p \frac{dT}{dt} \quad (28)$$

where the temperature variations rate  $\frac{dT}{dt}$  is constant as imposed by the ramp. We deduce then:

$$c_p = \frac{\phi}{m} \left( \frac{dT}{dt} \right)^{-1} \quad (29)$$

Resulting values of the effective  $c_p$  are represented in Fig. 10 as a function of temperature. Similar trends are observed for all protocols. For large temperature values (above 25 °C) the material is liquid, the heat capacity is quasi constant  $c_p = 2.13 \text{ kJ kg}^{-1} \text{ K}^{-1}$ . This value is recovered in the liquid phase for both cooling and heating experiments. Similarly, in the solid phase, i.e. for low temperature values (below 10°C) we obtain  $c_p = 2.74 \text{ kJ kg}^{-1} \text{ K}^{-1}$ . In the temperature range where solidification (fig. 10a) or melting (fig. 10b) occurs, variations in results are due to a competition between the kinetics of the phase change processes and the rate of temperature variations. This competition leads to a hysteresis in temperature when solidifying which corresponds to undercooling effects. These latter effects decrease with slow temperature variations. In the case of temperature steps, the melting is observed between 10°C and 22°C while the solidification occurs between 20°C and 10°C. Further differences between melting and freezing processes can be highlighted. Indeed, two distinct local maxima are observed during crystallization as the temperature decreases. These extrema are obtained for similar temperature values when the cooling protocol is long enough. Here,

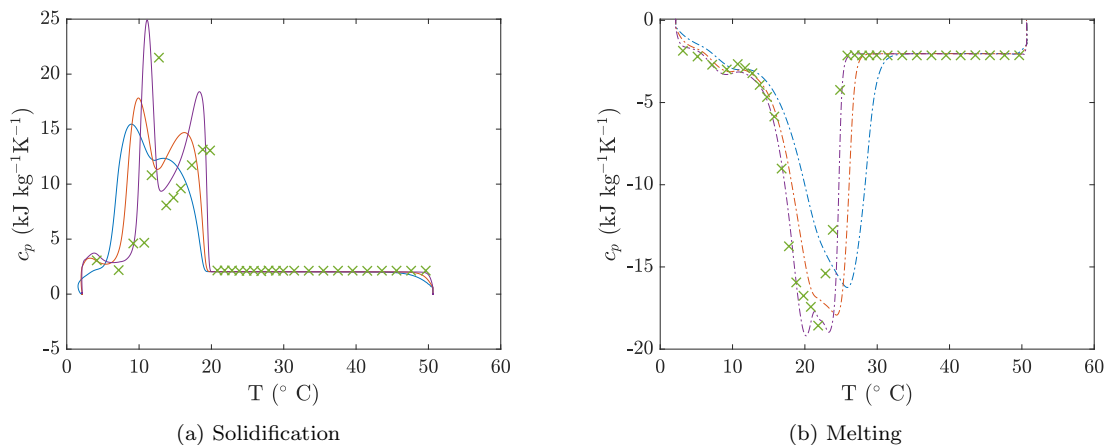


Figure 10: Effective  $c_p(T)$  evaluated during (a) solidification process and (b) melting process - for temperature variations of  $1^\circ\text{C}/\text{min}$  (Blue),  $0.5^\circ\text{C}/\text{min}$  (Red),  $0.2^\circ\text{C}/\text{min}$  (purple) and temperature steps (Green crosses)

extrema correspond to exothermal transformations correlated to structural modifications during crystallization [20, 21]. Whatever the protocol used, the integration of the only part due to phase transition in the effective heat capacity leads to a similar latent heat given by  $L_{solidification} = 130 \text{ kJ kg}^{-1}$ . Reciprocally, for the melting process, at least one extremal value in terms of  $c_p$  is also obtained. When the heating process is long enough ( $0.2^\circ\text{C}/\text{min}$ ), two local extrema can be observed but variations in their vicinity are smaller than in the case of the solidification process. Similarly, latent heat is evaluated and values obtained from different protocols converge to  $L_{melting} = 127 \text{ kJ kg}^{-1}$  which is close to the one obtained during the freezing process. Furthermore, our values are in very good agreement with the one proposed by Lane [19], that is to say  $127.2 \text{ kJ kg}^{-1}$ .

#### 4. Conclusion

In this study, a complete experimental characterization of polyethylene glycol, the PEG 600, in both liquid and solid phases was performed. The density was measured in the temperature range of  $21^\circ\text{C}$  to  $100^\circ\text{C}$ . The temperature increment involved in our measurements is small enough to provide a fit representing the density variations with temperature. It allows also to determine the volume expansion coefficient in the liquid phase with a good

accuracy. The density of solid phase has been measured using a pycnometer leading to  $\rho = 1510 \text{ kg m}^{-3}$  at  $0.5^\circ\text{C}$ . This value highlights a relative variation in density about 35% from the liquid to the solid phase since the density in the liquid phase is around  $\rho \approx 1100 \text{ kg m}^{-3}$ . It also highlights a quite large volume shrinkage when solidifying which could have a drastic consequence on thermal contact at interfaces. That could have a strong impact in any use of PEG in thermal energy systems. To our knowledge, this result has never been reported before in the literature. Similarly, the thermal conductivity of each liquid and solid phase has been measured by means of a steady state method and a transient hot needle method. The results obtained with both methods are in agreement with the few data available in the literature. The thermal conductivity of the solid phase was obtained using the transient needle probe to provide original data and fill the gaps in the literature. These characteristics will allow to bring new insights in terms of the PEG 600 behaviour at the phase transition in particular. Measurements performed with the differential scanning calorimeter enable to describe and quantify heat transfer and effective heat capacity of the PEG. Far from the phase transition range of temperatures, we obtain constant values of the specific heat capacity in each the solid and liquid phase. Phase transition occurs in the calorimeter within the temperature range  $10^\circ\text{C}$  to  $25^\circ\text{C}$  depending whether the PEG is cooled or heated. Undercooling effects lead to a hysteresis in the temperatures at which phase change occurs. These effects decrease as the cooling temperature rate is decreased. For all protocols, we obtain a similar value of the latent heat given by  $L_{melting}=127 \text{ kJ kg}^{-1}$ ,  $L_{solidification} = 130 \text{ kJ kg}^{-1}$ . More interestingly, we have observed several exothermic peaks during the freezing process highlighting some reorganizations within the internal structure of PEG aggregates or crystals or possibly within the chain conformation. The scope of our present study was not to investigate these small scales but only to provide thermal macroscopic properties as a first step. Explanations about the PEG crystallization are still controversial in the literature, we aim at investigating these scales in a future work. Moreover, at macroscopic scales, the knowledge of physical properties of the PEG would help to fully understand this material. In particular, we are investigating the rheological properties of the PEG in order to understand the coupling between thermodynamical and physical behaviours through the phase transition. For instance, that would complete some recent work proposed by Azri et al. [27].

## Appendix A. Estimation of the error due to steady-state contact resistances

During solidification the density varies leading generally to  $\rho_l < \rho_s$ , meaning that the volume decreases with the temperature. It results in an air layer of thickness  $\epsilon$  between the solid and the inner heating tube of diameter  $r_0$ . Thus, one can write:

$$\rho_l \pi (r_1^2 - r_0^2) = \rho_s \pi [r_1^2 - (r_0 + \epsilon)^2] \quad (\text{A.1})$$

leading to

$$\epsilon = [r_1^2 - \frac{\rho_l}{\rho_s} (r_1^2 - r_0^2)]^{0.5} - r_0$$

The thermal resistance between the two tubes is:

$$R = \frac{\ln\left(\frac{r_1}{r_1 - r_0 - \epsilon}\right)}{2\pi\lambda} + \frac{\ln\left(\frac{r_0 + \epsilon}{r_0}\right)}{2\pi\lambda_{air}} = \frac{\ln\left(\frac{r_1}{r_0}\right)}{2\pi\lambda_m} \quad (\text{A.2})$$

Hence  $\lambda_m$  is the measured value of the thermal conductivity and  $\lambda$ , the thermal conductivity of the sample. We deduce :

$$\lambda_m = \frac{\ln\left(\frac{r_1}{r_0}\right)}{\frac{\ln\left(\frac{r_1}{r_1 - r_0 - \epsilon}\right)}{\lambda} + \frac{\ln\left(\frac{r_0 + \epsilon}{r_0}\right)}{2\pi\lambda_{air}}} \quad (\text{A.3})$$

The values of the parameters for the device used are:  $r_0 = 2.75$  mm ;  $r_1 = 6$  mm; with a estimated value for the solid of

$\lambda = 0.27$  W m<sup>-1</sup> K<sup>-1</sup>, we can calculate the value  $\lambda_m$  that we would have been measured with the hot tube steady state. For a value  $\rho_l/\rho_s = 0.75$ , the calculation leads to  $\lambda_m = 0.19$  W m<sup>-1</sup> K<sup>-1</sup>, which is 30% less than the actual value. This steady-state measuring device used in this study is unsuitable for measuring the thermal conductivity of a solid obtained by solidification of a liquid initially filling the device. For this reason, it is preferable to measure the thermal conductivity of a solid PCM using a transient measurement device where contact resistances have no influence on the conductivity estimate.

## Acknowledgments

Financial supports have been brought to this work by the operation “STOCK’NRJ” co-financed by the European Union within the framework of the Program FEDER-FSE Lorraine and Massif des Vosges 2014-2020.

## References

- [1] M. Kobayashi, T. Koide, S.-H. Hyon, Tribological characteristics of polyethylene glycol (peg) as a lubricant for wear resistance of ultra-high-molecular-weight polyethylene (uhmwpe) in artificial knee joint, *Journal of the mechanical behavior of biomedical materials* 38 (2014) 33–38.
- [2] K. Bjugstad, D. Redmond Jr, K. Lampe, D. Kern, J. Sladek Jr, M. Mahoney, Biocompatibility of peg-based hydrogels in primate brain, *Cell transplantation* 17 (4) (2008) 409–415.
- [3] A. K. Jain, A. K. Goyal, N. Mishra, B. Vaidya, S. Mangal, S. P. Vyas, Peg-pla-peg block copolymeric nanoparticles for oral immunization against hepatitis b, *International journal of pharmaceutics* 387 (1-2) (2010) 253–262.
- [4] S. M. Baygi, S. Sadrameli, Thermal management of photovoltaic solar cells using polyethylene glycol 1000 (peg1000) as a phase change material, *Thermal Science and Engineering Progress* 5 (2018) 405–411.
- [5] F. Hamad, E. Egelle, K. Cummings, P. Russell, Investigation of the melting process of polyethylene glycol 1500 (peg 1500) in a rectangular enclosure, *International Journal of Heat and Mass Transfer* 114 (2017) 1234–1247.
- [6] J. Wang, M. Yang, Y. Lu, Z. Jin, L. Tan, H. Gao, S. Fan, W. Dong, G. Wang, Surface functionalization engineering driven crystallization behavior of polyethylene glycol confined in mesoporous silica for shape-stabilized phase change materials, *Nano Energy* 19 (2016) 78–87.
- [7] J. Yang, E. Zhang, X. Li, Y. Zhang, J. Qu, Z.-Z. Yu, Cellulose/graphene aerogel supported phase change composites with high thermal conductivity and good shape stability for thermal energy storage, *Carbon* 98 (2016) 50–57.

- [8] J. Jin, F. Lin, R. Liu, T. Xiao, J. Zheng, G. Qian, H. Liu, P. Wen, Preparation and thermal properties of mineral-supported polyethylene glycol as form-stable composite phase change materials (cpcms) used in asphalt pavements, *Scientific reports* 7 (1) (2017) 1–10.
- [9] Y. Zhou, X. Liu, D. Sheng, C. Lin, F. Ji, L. Dong, S. Xu, H. Wu, Y. Yang, Graphene oxide/polyurethane-based solid–solid phase change materials with enhanced mechanical properties, *Thermochimica Acta* 658 (2017) 38–46.
- [10] A. Sharma, V. V. Tyagi, C. Chen, D. Buddhi, Review on thermal energy storage with phase change materials and applications, *Renewable and Sustainable energy reviews* 13 (2) (2009) 318–345.
- [11] B. Zalba, J. M. Marin, L. F. Cabeza, H. Mehling, Review on thermal energy storage with phase change: materials, heat transfer analysis and applications, *Applied thermal engineering* 23 (3) (2003) 251–283.
- [12] M. Firoozzadeh, A. H. Shiravi, M. Shafiee, Experimental and Analytical Study on Enhancing Efficiency of the Photovoltaic Panels Using Polyethylene-Glycol 600 (PEG 600) as a Phase Change Material, *Iranian Journal of Energy and Environment* 10 (2019) 23–32. doi:10.5829/ijee.2019.10.01.04.
- [13] R. Velraj, R. Seeniraj, B. Hafner, C. Faber, K. Schwarzer, Heat transfer enhancement in a latent heat storage system, *Solar energy* 65 (3) (1999) 171–180.
- [14] Y. Kou, S. Wang, J. Luo, K. Sun, J. Zhang, Z. Tan, Q. Shi, Thermal analysis and heat capacity study of polyethylene glycol (peg) phase change materials for thermal energy storage applications, *The Journal of Chemical Thermodynamics* 128 (2019) 259–274.
- [15] C. Aucouturier, G. Roux-Desgranges, A. Roux, Excess molar volumes and excess molar heat capacities of (polyethylene glycols+ water) at temperatures between  $T = 278$  k and  $T = 328$  k, *The Journal of Chemical Thermodynamics* 31 (2) (1999) 289–300.
- [16] S. Trivedi, C. Bhanot, S. Pandey, Densities of {poly (ethylene glycol)+ water} over the temperature range (283.15 to 363.15) k, *The Journal of Chemical Thermodynamics* 42 (11) (2010) 1367–1371.

- [17] A. Singh, R. Walvekar, M. Khalid, W. Y. Wong, T. Gupta, Thermophysical properties of glycerol and polyethylene glycol (peg 600) based des, *Journal of Molecular Liquids* 252 (2018) 439–444.
- [18] Z. Mousavi, M. Pirdashti, A. A. Rostami, E.-N. Dragoi, Thermophysical properties analysis of poly (ethylene glycol) 600+ methanol, ethanol, 1-propanol, and 2-propanol binary liquid mixtures, *International Journal of Thermophysics* 41 (2) (2020) 1–26.
- [19] G. A. Lane, Low temperature heat storage with phase change materials, *International Journal of Ambient Energy* 1 (3) (1980) 155–168.
- [20] L. Yang, T. Smith, Melting and solidification behavior of blends of high density polyethylene with poly (butylene terephthalate), *Polymer Engineering & Science* 33 (21) (1993) 1426–1430.
- [21] A. Azri, P. Giamarchi, Y. Grohens, R. Olier, M. Privat, Polyethylene glycol aggregates in water formed through hydrophobic helical structures, *Journal of colloid and interface science* 379 (1) (2012) 14–19.
- [22] D. Fischer, Organisation de copolymères à blocs amphiphiles polyéthylène-b-polyéthylène glycol aux interfaces solides et liquides, Ph.D. thesis, Université de Haute Alsace-Mulhouse (2015).
- [23] D. D. Gray, A. Giorgini, The validity of the boussinesq approximation for liquids and gases, *International Journal of Heat and Mass Transfer* 19 (5) (1976) 545–551.
- [24] Y. Jannot, A. Degiovanni, Thermal properties measurement of materials, John Wiley & Sons, 2018.
- [25] J. Huetz, J.-P. Petit, Notions de transfert thermique par convection, *Techniques de l'Ingénieur (A1504A)* (Aug. 1990).
- [26] A. I. Brown, S. M. Marco, Introduction to heat transfer, 3rd Edition, Mc Graw-Hill Book Company, New York, 1958.
- [27] A. Azri, M. Privat, Y. Grohens, T. Aubry, Linear rheological properties of low molecular weight polyethylene glycol solutions, *Journal of colloid and interface science* 393 (2013) 104–108.